2009

Electronic inhomogeneity and Ag:Sb imbalance of Ag1−yPb18Sb1+zTe20 high-performance thermoelectrics elucidated by 125Te and 207Pb NMR

E. M. Levin
Ames Laboratory DOE

B. A. Cook
Ames Laboratory DOE

K. Ahn
Northwestern University

M. G. Kanatzidis
Northwestern University

Ames Laboratory DOE

Electronic inhomogeneity and Ag:Sb imbalance of Ag$_{1-y}$Pb$_{18}$Sb$_{1+z}$Te$_{20}$ high-performance thermoelectrics elucidated by ^{125}Te and ^{207}Pb NMR

E. M. Levin,[1,2,*,†] B. A. Cook,[1] K. Ahn,[3] M. G. Kanatzidis,[3] and K. Schmidt-Rohr[1,4,*,‡]

[1]*Ames Laboratory DOE, Ames, Iowa 50011, USA*
[2]*Department of Physics and Astronomy, Iowa State University, Ames, Iowa 50011, USA*
[3]*Department of Chemistry, Northwestern University, 2145 Sheridan Road, Evanston, Illinois 60208, USA*
[4]*Department of Chemistry, Iowa State University, Ames, Iowa 50011, USA*

Using magic-angle spinning ^{125}Te and ^{207}Pb NMR, we have discovered the presence of two phases of approximately tenfold different free-electron concentration, n, in high-performance thermoelectrics Ag$_{1-y}$Pb$_{18}$Sb$_{1+z}$Te$_{20}$ ("LAST-18"), proven by pairs of Knight-shifted NMR peaks and biexponential spin-lattice relaxation. The ratio of the phases is typically 2:1 with $n \approx 2 \times 10^{19}$ cm^{-3} and 0.2×10^{19} cm^{-3}, respectively, determined from the spin-lattice relaxation times. ^{125}Te NMR spectra show that both phases contain similar concentrations of Sb. The low-n component is assigned to Ag-rich regions with Ag-Sb pairing (but not AgSbTe$_2$), the dominant high-n component to PbTe:Sb resulting from the excess of Sb relative to Ag. The electronic inhomogeneity observed here must be considered in the search for a better understanding of high-performance thermoelectric materials.

PACS number(s): 72.20.Pa, 76.60.−k

I. INTRODUCTION

Direct conversion of heat to electricity based on the thermoelectric or Seebeck effect is an attractive route to alternative electrical power generation.[1–3] It requires thermoelectric materials with high figures of merit, $ZT = (S^2 \sigma T)/k$, where T, S, σ, and k are the temperature, Seebeck coefficient, electrical, and thermal conductivity, respectively. One of the most promising types of bulk thermoelectrics is Ag$_{1-y}$Pb$_{18}$Sb$_{1+z}$Te$_{20}$, commonly referred to as LAST-18, with a reported figure of merit $ZT \sim 1.7$ at 800 K, which is exceptionally high for bulk materials.[4–7] The high ZT can be attributed mainly to the very low lattice thermal conductivity of the system, which in turn is believed to be a consequence of nanoscale compositional inhomogeneities that increase phonon scattering. However, in spite of many experimental and theoretical studies,[8–12] both the composition and the electronic nature of these important materials remain poorly understood. It has been shown that the LAST system is in fact compositionally inhomogeneous, using pair distribution function analysis based on total scattering.[8] Recently, the formation of Ag$_2$Te (Ref. 9) and AgSbTe$_2$ (Ref. 10) nanoinclusions was proposed. In addition, scanning Seebeck microprobe measurements have indicated that LAST materials are in fact electronically inhomogeneous on the millimeter scale, despite appearing homogeneous to x-ray diffraction.[11]

Therefore, reliable, high-resolution intrinsic probes of the local structure as well as the charge-carrier concentration and its distribution in complex thermoelectric tellurides are urgently needed. Nuclear magnetic resonance (NMR) is an emergent method with unique capabilities to fill this need. Ag$_{1-y}$Pb$_m$Sb$_{1+z}$Te$_{2+m}$ alloys contain several NMR-active isotopes, including two spin-1/2 nuclei (^{125}Te and ^{207}Pb) of high sensitivity. NMR can identify different tellurides based on ^{125}Te chemical shifts, even for inclusions of nanometer dimensions since nuclear spins are local probes.

Here, we report upper limits, from ^{125}Te NMR, to the amounts of various suggested nanoinclusions[9,10] in LAST-18

(Ref. 4) and show that most Sb is dissolved in the PbTe matrix. Further, we use NMR to determine the concentration of free electrons, n, reflected in Knight shifts of the ^{125}Te and ^{207}Pb resonance frequencies and in the strong n dependence of the spin-lattice relaxation times, $T_{1,\text{Te}}$ and $T_{1,\text{Pb}}$, driven by hyperfine interactions of the nuclear spins with the spin-polarized charge carriers. In neat PbTe, these relations have been documented quantitatively.[13–15] Through the spectrum of Knight shifts and the distribution of T_1 relaxation times, the distribution $P(n)$ can be measured and related to compositional inhomogeneities.[16] Our results imply that a deeper understanding of the LAST system will require not only awareness of the compositional but also of the electronic-carrier inhomogeneities and their interrelationships.

II. EXPERIMENT

A. Samples synthesis

Samples of Ag$_{0.53}$Pb$_{18}$Sb$_{1.2}$Te$_{20}$ and Ag$_{0.86}$Pb$_{18}$SbTe$_{20}$ (LAST-18) were synthesized from the constituent elements (see Refs. 4–6). Thermal treatments were as follows: quenching from 1273 K (LAST-18-q), followed by annealing at 723 K for 2 days (LAST-18-qa); slow cooling to 973 K (solid state), then quenching to ambient temperature (LAST-18-sq); and slow cooling from 1273 to 773 K in 72 h (LAST-18-sc). The composition and room-temperature Seebeck coefficient of $S = -150$ μV/K measured for LAST-18-qa and LAST-18-sc is similar to that of the high-ZT LAST-18 materials whose electric and transport properties have been described in Ref. 4. The microstructure of sample LAST-18-sc has been analyzed in detail in Refs. 4 and 9. The Ag$_{0.86}$Pb$_{18}$SbTe$_{20}$ sample (LAST-18-Ag$_{0.86}$) was cooled from 1223 to 723 K and then furnace cooled. Coarse powders of these materials, produced manually using a mortar and pestle, were packed into zirconia rotors for magic-angle spin-

ning (MAS) NMR. Two different samples of PbTe with different free-electron concentration were measured for reference, one (termed PbTe-n19) with $n = 2 \times 10^{19}$ cm^{-3} according to Hall-effect measurements and the other (PbTe-n18) with a lower $n = 1.2 \times 10^{18}$ cm^{-3} according to Seebeck-effect measurements.

B. Nuclear magnetic resonance

Solid-state NMR experiments were run on a Bruker Biospin (Billerica, MA) DSX-400 spectrometer (magnetic field of 9.3900 T) at 126 MHz for ^{125}Te and 84 MHz for ^{207}Pb, at ambient temperature. A 2.5 mm probe head was used at 22 kHz MAS for ^{125}Te NMR, a 4 mm Bruker probe head at 8 kHz MAS for ^{207}Pb NMR experiments. Sample masses were ~30 and 300 mg for 2.5 and 4 mm zirconia rotors, respectively. The $\pi/2$ pulse length was 2.6 μs in either probe head. Signals were detected after a Hahn echo generated by a 2 μs$-t_r-$3.8 μs$-t_r$ two-pulse sequence, where t_r denotes a rotation period. This provides a significantly larger excitation width than the regular $\pi/2-t_r-\pi-t_r$ sequence.[17] The second pulse and receiver phase were cycled according to the EXORCYCLE scheme,[18] which eliminates spectral distortions that would otherwise arise from the reduced pulse lengths. Measuring times were around 3 h for the spectra of the short T_1 and 12–25 h for the long-T_1 components. The longest-signal averaging was needed for the T_1-filtered spectra, which were obtained with 3–5 s recycle delays and 0.3–0.6 s T_1 filtering of magnetization stored alternately along $+z$ and $-z$.[19] T_1 relaxation was measured by observing magnetization recovery $M(t_{rec})$ after four-pulse saturation. ^{125}Te NMR chemical shifts were referenced to Te(OH)$_6$ in solution[17] via solid TeO$_2$ at +750 ppm as a secondary reference. ^{207}Pb NMR chemical shifts were referenced to (CH$_4$)$_4$Pb in solution[17] via solid Pb(NO$_3$)$_2$ at -3500 ppm as a secondary reference.

Challenges arose initially from relatively wide ranges of potential resonance frequencies (>4000 ppm or 500 kHz), exceeding pulse bandwidths, combined with significant line broadening and sizeable chemical-shift anisotropies (~40 kHz in LAST-18), which preclude signal detection by simple broadband one-pulse excitation.

III. RESULTS AND DISCUSSION

A. ^{125}Te NMR

Figure 1 shows ^{125}Te NMR spectra of the quaternary LAST-18-sq ("solid-quenched") material and of related binary and ternary reference compounds. Comparison of the static and 22 kHz MAS spectra of LAST-18-sq in Figs. 1(a) and 1(b) demonstrates that fast MAS provides crucial line narrowing. The spectrum in Fig. 1(b) clearly shows a large and a small peak. These can be assigned to Te surrounded by six Pb and to Te bonded to Sb, respectively, based on comparison with the spectra of Sb-doped PbTe and of neat PbTe, see Figs. 1(c) and 1(d). Figure 1(e) displays ^{125}Te MAS NMR peak positions of several relevant model compounds. AgSbTe$_2$ has a broad resonance near -1000 ppm while Sb$_2$Te$_3$ resonates around -400 ppm. On the right, near
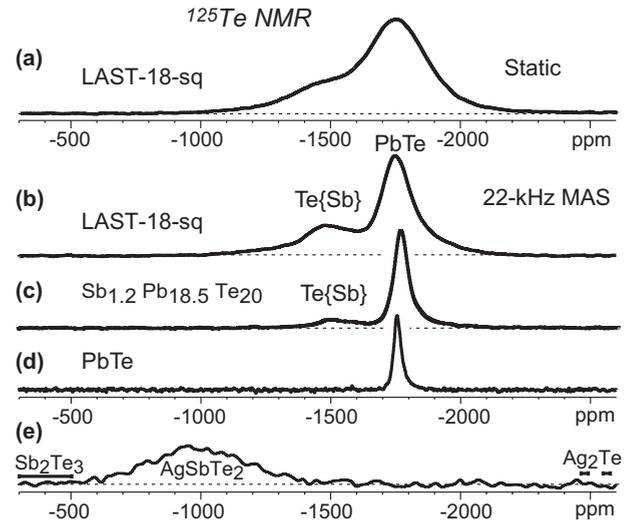

FIG. 1. ^{125}Te NMR spectra (a) of Ag$_{0.53}$Pb$_{18}$Sb$_{1.2}$Te$_{20}$, LAST-18-sq (see Table I); (b) also of LAST-18-sq but measured at 22 kHz MAS; (c) of Sb$_{1.2}$Pb$_{18.5}$Te$_{20}$; (d) of PbTe; and (e) of AgSbTe$_2$. Peak positions of Sb$_2$Te$_3$ and Ag$_2$Te are also indicated.

-2500 ppm, the peak positions of two modifications of Ag$_2$Te are indicated.

We also performed NMR experiments on LAST-18-qa ("quenched and annealed") and on LAST-18-Ag$_{0.86}$ (Ag$_{0.86}$Pb$_{18}$SbTe$_{20}$) with the specific aim of detecting low Ag$_2$Te, AgSbTe$_2$, and Sb$_2$Te$_3$ peaks. No such signals were observed above the noise level, limiting the fractions of Te in Ag$_2$Te, Sb$_2$Te$_3$, and AgSbTe$_2$ to <0.5%, <1.5%, and <1.5%, respectively. This indicates that the theoretically proposed formation of AgSbTe$_2$ inclusions in AgPb$_m$SbTe$_{2+m}$ (Ref. 10) is not significant in our LAST-18 materials. The clear peak of Te bonded to Sb in our spectra near -1550 ppm suggests that Sb atoms are dissolved in the PbTe matrix of LAST-18 at $x > 4\%$ [with x defined by (PbTe)$_{1-x}$(AgSbTe$_2$)$_{x/2}$ as in Ref. 10], which is not in agreement with the calculated phase diagram of Ag and Sb substitution in PbTe, where $x < 1\%$ (Ref. 10); the observed change in the lattice parameter of PbTe with Ag,Sb doping[4,12,20] confirms our conclusion. This discrepancy might be related to the deviation of our high-ZT LAST materials[4] from the exact AgPb$_m$SbTe$_{2+m}$ stoichiometry assumed in Ref. 10.

Information on the free-electron concentration and its inhomogeneity in high-ZT LAST materials are obtained from Fig. 2, which compares ^{125}Te NMR spectra of various LAST samples. The spectral patterns of LAST-18-sq and of Ag$_{0.86}$Pb$_{18}$SbTe$_{20}$ (LAST-18-Ag$_{0.86}$) in Fig. 2(a) are similar but shifted by ~200 ppm relative to each other and their T_1 relaxation times differ by more than two orders of magnitude. This is clearly a Knight shift of the resonance frequency with associated reduced T_1 relaxation time.[13] The resonance shift and the T_1 difference is mirrored in the different peak position and T_1 relaxation time of two neat PbTe samples with a 20-fold difference in carrier concentration n [see Fig. 2(b)]. For three samples of Ag$_{0.53}$Pb$_{18}$Sb$_{1.2}$Te$_{20}$ (a composition with high $ZT > 1.4$),[9] four distinct resonances can be revealed by spectral editing based on differences in T_1
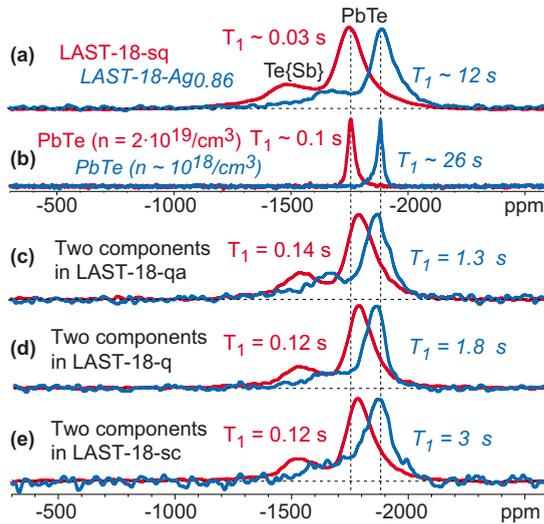
FIG. 2. (Color online) 22 kHz MAS ^{125}Te NMR spectra of (a) (red, left trace) LAST-18-sq and (blue, right trace) $Ag_{0.86}Pb_{18}SbTe_{20}$. T_1 relaxation times are given next to the spectra. (b) Spectra of two PbTe samples, red, left trace: high n and blue, right trace: low n. (c) Short (red, left trace) and long (blue, right trace) T_1 components of quenched and annealed $Ag_{0.53}Pb_{18}Sb_{1.2}Te_{20}$, LAST-18-qa, after 50 ms recycle delay and a 0.6 s T_1 filter with 3 s recycle delay, respectively. Peaks are scaled to equal height. (d) Same material as in (c) but without annealing after quenching. (e) Same material as in (c) but slowly cooled from 1273 to 773 K.
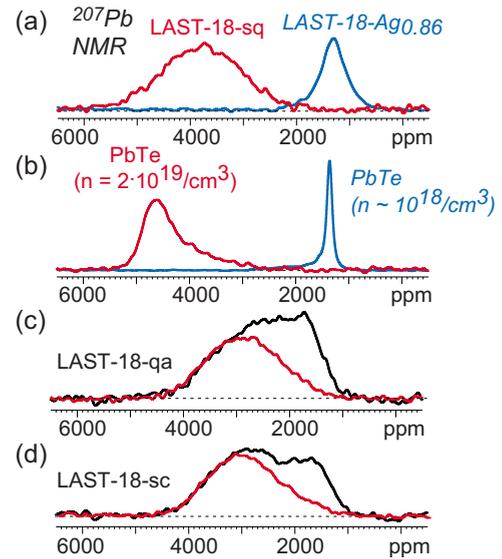

FIG. 3. (Color online) ^{207}Pb NMR spectra. (a) Red, left trace: spectrum of LAST-18-sq measured at 8 kHz MAS using a two-pulse echo sequence with 2 μs excitation and 3.8 μs refocusing pulses, after 0.1 s recycle delay; blue, right trace: corresponding spectrum of $Ag_{0.86}Pb_{18}SbTe_{20}$, after a 10 s recycle delay. (b) Spectra of PbTe for reference. Red, left trace: PbTe-n19, with 1 s recycle delay. Blue, right trace: PbTe-n18, with 10 s recycle delay. (c) Black, top trace: full spectrum of LAST-18-qa, obtained with 1 s recycle delay. Red, lower trace: short-T_1 component measured with 30 ms recycle delay. (d) Same for LAST-18-sc.

relaxation times, see Figs. 2(c)–2(e). The presence of distinct long- and short-T_1 subspectra demonstrates inhomogeneity of the electron concentrations within each of these samples.

B. ^{207}Pb NMR

Detailed NMR studies of n- and p-type PbTe have shown that Knight shifts of ^{207}Pb have the same sign as those of ^{125}Te and are $\sim$20-fold greater.[13,14] The expected large ^{207}Pb NMR Knight shifts and corresponding short T_1 values are observed for four LAST-18 materials and the two PbTe samples (see Fig. 3), exhibiting a similar pattern as the ^{125}Te NMR data of Fig. 2. Figures 3(a) and 3(b) show that ^{207}Pb nuclei in LAST-18-sq and PbTe-n19 resonate at low frequency and have short T_1 relaxation times while the NMR signals of LAST-18-Ag$_{0.86}$ and PbTe-n18 appear at high frequency and exhibit long T_1 values. For quantifying the electron concentration, T_1 analysis is more suitable than Knight-shift measurement since T_1 values can be measured over more than three orders of magnitude and increase monotonously with p or n while the Knight shift reaches a maximum at high electron concentrations, $\sim$2$\times$10^{19} cm^{-3}.[15]

Comparison of spectra of LAST-18-qa and LAST-18-sc obtained with short and long recycle delays [see Figs. 3(c) and 3(d)], again shows two components with distinctly different T_1 relaxation times in each sample. As in ^{125}Te NMR, the longer T_1 is associated with a shift to lower frequency (to the right). The simple spectrum of LAST-18-Ag$_{0.86}$ in Fig. 3(a) confirms that the multiple T_1 components observed in the other LAST samples are not an artifact of the NMR

method but indeed reflect intrinsic inhomogeneity of those samples. Other ^{207}Pb NMR signals were not ($<$5%) observed within a 0.6 MHz range on either side of the LAST-18-qa spectrum (total range of 15 500 ppm). It is interesting to note that unlike the ^{125}Te spectrum, the ^{207}Pb spectrum is not expected to exhibit a resonance that is chemically shifted by bonding to Sb because Pb and Sb occupy the same sublattice and are thus separated by Te atoms.

C. Charge-carrier concentrations from NMR

The presence of two distinct tellurium environments, characterized by a major difference in charge-carrier concentrations, in LAST-18-q, LAST-18-qa, and LAST-18-sc is confirmed by the biexponential behavior of the ^{125}Te and ^{207}Pb T_1 relaxation curves presented in Fig. 4. Fits to these relaxation curves provide the two relaxation times and the fractions, f_A and f_B, of the two components (which are constrained to be the same in ^{125}Te as in ^{207}Pb relaxation), as listed in Table I.

The observed ^{207}Pb and ^{125}Te T_1 relaxation times can be converted into carrier concentrations, as shown in Fig. 5, using plots of ^{207}Pb and ^{125}Te 1/T_1 relaxation rates vs n for four reference and two LAST-18 samples. ^{207}Pb relaxation data for our two PbTe samples, for LAST-18-Ag$_{0.86}$, as well as for two PbTe samples from Alexander et al.[15] with different n fall close to the same straight line in the log-log plots of Fig. 5. This enables us to estimate the carrier concentrations for each of the two T_1 components in each LAST-18 sample.
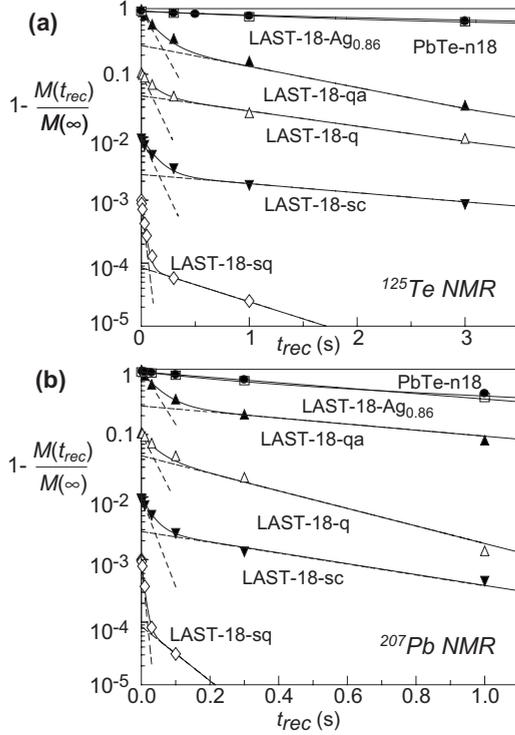
FIG. 4. (a) ^{125}Te and (b) ^{207}Pb spin-lattice (T_1) relaxation curves of PbTe-based thermoelectric materials, in semilogarithmic plots of the normalized signal intensity after saturation recovery for a time t_{rec}. Top three curves: PbTe-n18, $Ag_{0.86}Pb_{18}SbTe_{20}$, and LAST-18-qa; bottom three curves, successively shifted down by one decade: LAST-18-q, LAST-18-sc, and LAST-18-sq. The solid lines are biexponential fits with the two components indicated by straight dashed lines.
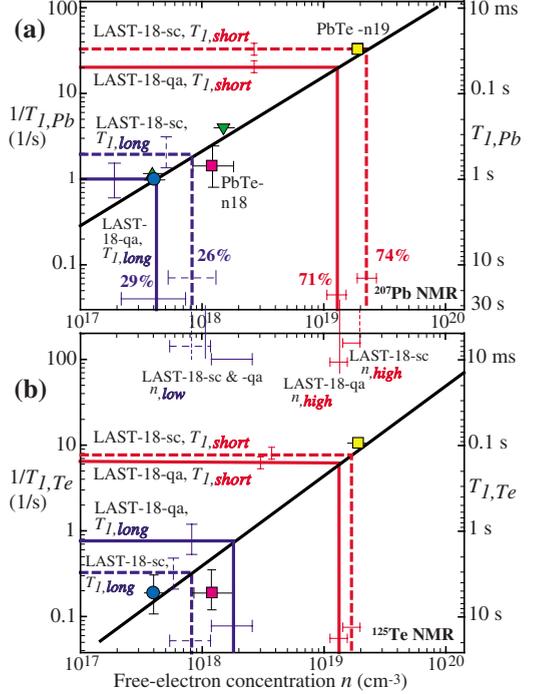

FIG. 5. (Color online) Determination of free-electron concentration n from spin-lattice relaxation rates $1/T_1$ for LAST-18-sc and LAST-18-qa samples. Data points from our two PbTe samples and from LAST-18-Ag$_{0.86}$ (filled dark circle) provide calibration curves (black diagonal lines). For ^{207}Pb data, two data points (labeled PbTe-1 and PbTe-2) for PbTe from Ref. 15 are also shown, as filled triangles. Measured T_1 relaxation times of LAST-18 materials (LAST-18-sq, dashed lines, and LAST-18-q, solid lines) can then be converted into n values. (a) ^{207}Pb data. (b) Corresponding ^{125}Te data. Averaged n values for the two environments in each of the two samples are shown in the center of the figure together with their volume fractions.

D. Origin of electronic inhomogeneity

What gives rise to the inhomogeneity of the electron concentration observed in the high-*ZT* LAST-18 materials? The charge-carrier concentration of PbTe-based materials depends sensitively on their composition. Neat PbTe is a self-doping narrow-band (0.26–0.3 eV) semiconductor with n-type conductivity resulting from Pb excess (Te vacancies) and p-type from Te excess (Pb vacancies).[21,22] Doping with Sb, an electron donor on the Pb sublattice, results in the

For instance, the two $1/T_1$ values of LAST-18-sc correspond to $n = 0.8 \times 10^{18}$ and 20×10^{18} cm^{-3}. In each of the four LAST-18 samples studied (see Table I), the n values in the two environments differ by more than an order of magnitude and are present in a $\sim$30:70 ratio on average. This illustrates the unique capabilities of NMR for quantitatively probing the distribution of the charge-carrier concentration, $P(n)$, while Hall- and Seebeck-effect measurements provide only a bulk average. Unlike Hall-effect measurements, NMR is a contactless technique and can interrogate samples of random shapes including polycrystalline and powdered materials.

TABLE I. Synthesis conditions of four $Ag_{0.53}Pb_{18}Sb_{1.2}Te_{20}$ (LAST-18-...) materials, two-component fit parameters for ^{125}Te and ^{207}Pb spin-lattice relaxation, and charge-carrier concentrations n of PbTe-based thermoelectric materials. The LAST-18-sc material, with $n = 18 \times 10^{18}$ cm^{-3} from Hall effect, is the same as studied in Ref. 9.

LAST-18-...	Synthesis	f_A	f_B	$T_{1,A,Te}$ (s)	$T_{1,B,Te}$ (s)	$T_{1,A,Pb}$ (s)	$T_{1,B,Pb}$ (s)	n_A from NMR (cm^{-3})	n_B from NMR (cm^{-3})
-sc (slow cooled)	1272–773 K in 72 h	0.74	0.26	0.12	3.0	0.03	0.5	$(20 \pm 6) \times 10^{18}$	$(0.8 \pm 0.4) \times 10^{18}$
-q (quenched)	1273 K quenched	0.54	0.46	0.12	1.8	0.04	0.31	$(16 \pm 4) \times 10^{18}$	$(1.6 \pm 0.5) \times 10^{18}$
-qa (quenched and annealed)	-"- and annealed at 723 K	0.71	0.29	0.14	1.3	0.05	1.0	$(13 \pm 4) \times 10^{18}$	1.1 $(0.4$–$2.4) \times 10^{18}$
-sq (solid quenched)	973 K quenched	0.91	0.09	0.03	0.8	0.008	0.1	$(80 \pm 20) \times 10^{18}$	$(4 \pm 2) \times 10^{18}$

expected increased n-type carrier concentration.[23] In $Ag_{0.53}Pb_{18}Sb_{1.2}Te_{20}$, this n-type doping apparently overcomes the effect of the 1.4% Te excess [20 Te atoms: $(0.53 + 1.2 + 18 = 19.73)$ atoms on the Pb sublattice]. By contrast, Ag is an electron acceptor;[24] indeed, in the LAST-18-$Ag_{0.86}$ sample with the higher Ag concentration studied here, a low $n = 4 \times 10^{17}$ cm^{-3} was found.

The matching relative peak intensities in the pairs of long- and short-T_1 signals in Figs. 2(c) and 2(d) show similar levels of Sb incorporation in the high- and low-n phases of high-ZT LAST-18. Thus, the explanation should be sought in the distribution of Ag. Indeed, the high-ZT LAST materials do not have the "ideal" 1:1 Ag:Sb ratio but are deficient in Ag.[4] Nevertheless, Ag is crucial in increasing the solubility of Sb in PbTe, which is otherwise limited at <3 at. %.[24] This enhancement is confirmed by the greatly increased NMR signal of Te bonded to Sb in LAST-18-sc $(Ag_{0.53}Pb_{18}Sb_{1.2}Te_{20})$ compared to the corresponding Sb-doped PbTe $(Sb_{1.2}Pb_{18.53}Te_{20})$, see Figs. 1(b) and 1(c). This shows that Sb and Ag interact in the PbTe matrix, likely forming Ag-Sb pairs or somewhat larger clusters.[5,25]

Considering the excess of Sb over Ag in high-ZT LAST-18, the following picture of the electronic inhomogeneities emerges: in the phase with Ag-Sb pairs, Ag as an electron acceptor decreases the free-electron concentration (note also that $AgSbTe_2$ is a p-type material).[26] This low-n component accounts for $(1-y)/(1+z) = 0.53/1.2 = 44\%$ of all Sb and maybe less if some Ag is incorporated into Ag_2Te inclusions as reported by TEM.[9] The remaining Sb, >56%, forms a ternary PbTe:Sb alloy of high n due to n-type doping by Sb alone. This analysis also explains the low n (and poorer thermoelectric properties) of LAST-18 with a 1:1 Ag:Sb ratio[4,20] and the less inhomogeneous, low n of our LAST-18-$Ag_{0.86}$ with its nearly balanced, $(1-y)/(1+z) = 0.86:1$ Ag:Sb ratio. It highlights that simulations of 1:1 Ag:Sb LAST systems[9,20] are unlikely to reveal the origins of the high ZT of our LAST materials since the 1:1 systems in fact do not have a high ZT.[4,20] Rather, high-ZT LAST-18 appears to be predominantly a ternary PbTe:Sb material of high n, interspersed with regions rich in Ag-Sb pairs and low n. In addition, Ag_2Te nanoparticles have been detected by electron-beam methods,[9] though their volume fraction must be minor (<2%), due to the small Ag content.

The observed electronic inhomogeneity may result in strong energy-dependent electron scattering and an enhancement of ZT of narrow-gap degenerate semiconductors; such a mechanism was discussed recently for a model of metal/semiconductor interfaces formed by metallic nanoinclusions in PbTe (Ref. 27) and may also be important in LAST-18 materials. In addition, some contributions to the electronic inhomogeneity observed by NMR can arise from quasilocalized electron states near the Fermi level, which have been discussed for LAST-18 materials in Ref. 5. Both hypotheses need to be investigated further.

IV. CONCLUSIONS

This study has revealed electronic inhomogeneities in high-ZT LAST-18 thermoelectrics, with tenfold different charge-carrier concentration, and linked these to the Ag:Sb imbalance characteristic of high-ZT LAST-18 materials. Further, it has shown that Sb atoms are dissolved in the lattice of both phases while Sb_2Te_3, $AgSbTe_2$, or Ag_2Te inclusions are not detected in significant concentration. This demonstrates that high-resolution ^{125}Te NMR can provide important insights into the local structure and charge-carrier concentration of complex tellurides. Our study challenges the general assumption that thermoelectric materials are electronically homogeneous and illustrates the limitations of charge-carrier concentration measurements via Hall or Seebeck effect, which provide only a bulk average of what might be spatially varying carrier concentrations. The observed electronic inhomogeneity may result in strong energy-dependent electron scattering and an enhancement of ZT. It certainly needs to be considered when attempting to develop a deeper understanding of the factors determining ZT in nanostructured degenerate semiconductors.

ACKNOWLEDGMENTS

*Corresponding author.

†levin@iastate.edu

‡srohr@iastate.edu

[1] R. F. Service, Science **306**, 806 (2004).

[2] M. S. Dresselhaus, G. Chen, M. Y. Tang, R. Yang, H. Lee, D. Wang, Z. Ren, J.-P. Fleurial, and P. Gogna, Adv. Mater. **19**, 1043 (2007).

[3] L. E. Bell, Science **321**, 1457 (2008).

[4] K. F. Hsu, S. Loo, F. Guo, W. Chen, J. S. Dyck, C. Uher, T. Hogan, E. K. Polychroniadis, and M. G. Kanatzidis, Science **303**, 818 (2004).

[5] D. Bilc, S. D. Mahanti, K.-F. Hsu, E. Quarez, R. Pcionek, and M. G. Kanatzidis, Phys. Rev. Lett. **93**, 146403 (2004).

[6] D. I. Bilc, S. D. Mahanti, and M. G. Kanatzidis, Phys. Rev. B **74**, 125202 (2006).

[7] G. J. Snyder and E. S. Toberer, Nature Mater. **7**, 105 (2008).

[8] H. Lin, E. S. Bozin, S. J. L. Billinge, E. Quarez, and M. G. Kanatzidis, Phys. Rev. B **72**, 174113 (2005).

[9] B. A. Cook, M. J. Kramer, J. L. Harringa, M.-K. Han, D.-Y. Chung, and M. G. Kanatzidis, Adv. Funct. Mater. **19**, 1254 (2009).

[10] S. V. Barabash, V. Ozolins, and C. Wolverton, Phys. Rev. Lett. **101**, 155704 (2008).

[11] N. Chen, F. Gascoin, G. J. Snyder, E. Muller, G. Karpinski, and C. Stiewe, Appl. Phys. Lett. **87**, 171903 (2005).

[12] E. Quarez, K.-F. Hsu, R. Pcionek, N. Frangis, E. K. Polychroniadis, and M. G. Kanazidis, J. Am. Chem. Soc. **127**, 9177 (2005).

[13] S. D. Senturia, A. C. Smith, C. R. Hewes, J. A. Hofmann, and P. L. Sagalyn, Phys. Rev. B **1**, 4045 (1970).

[14] C. R. Hewes, M. S. Adler, and S. D. Senturia, Phys. Rev. B **7**, 5195 (1973).

[15] M. N. Alexander, P. L. Sagalyn, S. D. Senturia, and C. R. Hewes, J. Nonmet. **1**, 251 (1973).

[16] J. P. Yesinowski, A. P. Purdy, H. Wu, M. G. Spencer, J. Hunting, and F. J. DiSalvo, J. Am. Chem. Soc. **128**, 4952 (2006).

[17] I. Orion, J. Rocha, S. Jobic, V. Abadie, R. Brec, C. Fernandez, and J.-P. Amoureux, J. Chem. Soc. Dalton Trans. **1997**, 3741.

[18] G. Bodenhausen, R. Freeman, and D. L. Turner, J. Magn. Reson. (1969-1992) **27**, 511 (1977).

[19] D. A. Torchia, J. Magn. Reson. (1969-1992) **30**, 613 (1978).

[20] A. Kosuga, K. Kurosaki, H. Muta, and S. Yamanaka, in Proceedings of the 24th International Conference on Thermoelectrics, 19–23 June, 2005 (IEEE, New Jersey), p. 45.

[21] C. R. Hewes, M. S. Adler, and S. D. Senturia, J. Appl. Phys. **44**, 1327 (1973).

[22] S. Ahmad, S. D. Mahanti, K. Hoang, and M. G. Kanatzidis, Phys. Rev. B **74**, 155205 (2006).

[23] T. Su, P. Zhu, H. Ma, G. Ren, J. Guo, Y. Imai, and X. Jia, J. Alloys Comp. **422**, 328 (2006).

[24] T. Ikeda, S. M. Haile, V. A. Ravi, H. Azizgolshani, F. Gascoin, and G. J. Snyder, Acta Mater. **55**, 1227 (2007).

[25] H. Hazama, U. Mizutani, and R. Asahi, Phys. Rev. B **73**, 115108 (2006).

[26] H. Wang, J.-F. Li, M. Zou, and T. Sui, Appl. Phys. Lett. **93**, 202106 (2008).

[27] S. V. Faleev and F. Leonard, Phys. Rev. B **77**, 214304 (2008).